Article

Cell Reports

Cell of Origin Links Histotype Spectrum to Immune Microenvironment Diversity in Non-small-Cell Lung Cancer Driven by Mutant *Kras* and Loss of *Lkb1*

Graphical Abstract

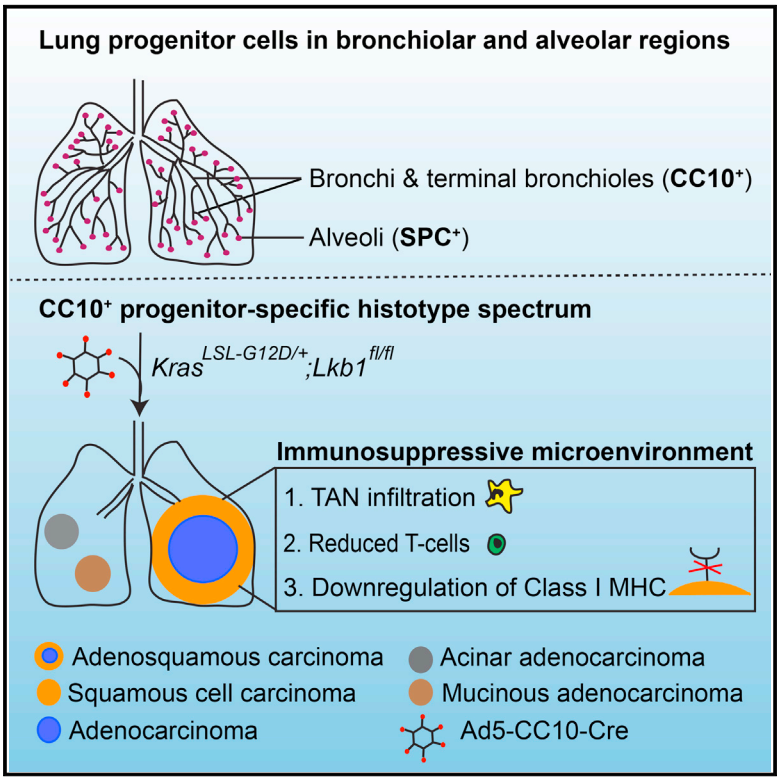

Highlights

- Cell of origin crucially defines tumor proliferation and the histopathology spectrum
- CC10^{+} cells are the predominant progenitors of ASC tumors in *Kras*;*Lkb1* mice
- CC10^{+} cells give rise to pure mucinous and acinar adenocarcinoma histotypes
- ASCs exhibit a histotype-specific immunosuppressive microenvironment

Authors

Ashwini S. Nagaraj, Jenni Lahtela, Annabrita Hemmes, ..., Mikko I. Mäyränpää, Katja Närhi, Emmy W. Verschuren

Correspondence

emmy.verschuren@helsinki.fi

In Brief

Nagaraj et al. demonstrate that the cell of origin defines the NSCLC histopathology spectrum and associated immune microenvironment upon the expression of *Kras*^{G12D} and loss of the tumor suppressor *Lkb1*. Significantly, the histopathology rather than the oncogenotype determined immune signatures, suggesting that a deeper understanding of histotype-dependent features is important for clinical decision-making.

Accession Numbers

GSE69552

Nagaraj et al., 2017, Cell Reports *18*, 673–684
January 17, 2017
http://dx.doi.org/10.1016/j.celrep.2016.12.059

Cell Reports
Article

Cell of Origin Links Histotype Spectrum to Immune Microenvironment Diversity in Non-small-Cell Lung Cancer Driven by Mutant *Kras* and Loss of *Lkb1*

Ashwini S. Nagaraj,[1,5] Jenni Lahtela,[1,5] Annabrita Hemmes,[1] Teijo Pellinen,[1] Sami Blom,[1] Jennifer R. Devlin,[1] Kaisa Salmenkivi,[2] Olli Kallioniemi,[1,4] Mikko I. Mäyränpää,[2,3] Katja Närhi,[1] and Emmy W. Verschuren[1,6,*]
[1]Institute for Molecular Medicine Finland (FIMM), University of Helsinki, Helsinki 00014, Finland
[2]HUSLAB, Division of Pathology, Helsinki University Hospital and University of Helsinki, Helsinki 00029, Finland
[3]Department of Pathology, University of Helsinki, Helsinki 00014, Finland
[4]Science for Life Laboratory, Department of Oncology and Pathology, Karolinska Institutet, 17165 Solna, Sweden
[5]Co-first author
[6]Lead Contact
*Correspondence: emmy.verschuren@helsinki.fi
http://dx.doi.org/10.1016/j.celrep.2016.12.059

SUMMARY

Lung cancers exhibit pronounced functional heterogeneity, confounding precision medicine. We studied how the cell of origin contributes to phenotypic heterogeneity following conditional expression of *Kras*^{G12D} and loss of *Lkb1* (*Kras*;*Lkb1*). Using progenitor cell-type-restricted adenoviral Cre to target cells expressing surfactant protein C (SPC) or club cell antigen 10 (CC10), we show that Ad5-CC10-Cre-infected mice exhibit a shorter latency compared with Ad5-SPC-Cre cohorts. We further demonstrate that CC10$^+$ cells are the predominant progenitors of adenosquamous carcinoma (ASC) tumors and give rise to a wider spectrum of histotypes that includes mucinous and acinar adenocarcinomas. Transcriptome analysis shows ASC histotype-specific upregulation of pro-inflammatory and immunomodulatory genes. This is accompanied by an ASC-specific immunosuppressive environment, consisting of downregulated MHC genes, recruitment of CD11b$^+$ Gr-1$^+$ tumor-associated neutrophils (TANs), and decreased T cell numbers. We conclude that progenitor cell-specific etiology influences the *Kras*;*Lkb1*-driven tumor histopathology spectrum and histotype-specific immune microenvironment.

INTRODUCTION

Lung cancers are relatively intractable with respect to detection and treatment, and pronounced histological and genomic heterogeneity compromises prognosis and treatment success (Chen et al., 2014). Factors contributing to tumor progression and therapy resistance may include genetic modifiers of signaling responses or stromal and immune regulators residing in the tumor-specific microenvironment. In addition, disease etiology can be influenced by niche-specific stem or progenitor cell functions (Leeman et al., 2014). In the murine lung, multiple stem/progenitor cell types have been identified based on their capacities to self-renew and/or differentiate following lung injury. This includes Krt5$^+$/p63$^+$ tracheal basal cells in the proximal airways, club cell antigen 10$^+$ (CC10$^+$) cells and dual CC10$^+$/surfactant protein C$^+$ (SPC$^+$) cells in the bronchioalveolar duct junctions (BADJs) in the distal airways, and SPC$^+$ alveolar type 2 (AT2) cells in the air spaces (Asselin-Labat and Filby, 2012). However, the relative roles of niche-specific progenitor cells in establishing potential histotype-specific tumor microenvironments remain poorly understood.

Clinically, non-small-cell lung cancer (NSCLC) accounts for around 85% of total lung cancers, with adenocarcinoma (AC; 40%) and squamous cell carcinoma (SCC; 30%) representing the major sub-histotypes (Travis et al., 2013). Lesions containing both AC and SCC features are classified as adenosquamous carcinoma (ASC; 0.4%–4%), a rare disease with poor prognosis (Nakagawa et al., 2003). NSCLC subtypes can be enriched for certain genetic alterations: activating mutations in *EGFR* or *KRAS* or loss-of-function mutations in serine/threonine kinase 11 (*STK11*, also known as *LKB1*) are common for AC and ASC, while loss-of-function mutations in *TP53*, *PTEN*, or *SOX2* amplification are common for SCC (Gridelli et al., 2015). *KRAS* mutation concurrent with loss of *LKB1* is common, detected in ~30% of NSCLC, and it represents a more aggressive metastasis-prone NSCLC subtype recapitulated by the preclinical *Kras*$^{G12D/+}$;*Lkb1*$^{fl/fl}$ (*Kras*;*Lkb1*) model (Calles et al., 2015; Ji et al., 2007). This highlights the relevance for a deeper understanding of potential histotype-specific etiologies of particularly the *Kras*;*Lkb1* subtype of lung cancers.

Recent insights into the cancer immunity cycle have identified promising approaches to targeting pro-tumorigenic immune cell populations or breaking tumor-elicited checkpoints to induce anti-tumor cytotoxic T cell responses (Chen and Mellman, 2013). Immunomodulatory therapies are particularly promising

for lung cancer since (1) these may functionally bypass acquired drug resistance caused by pronounced tumor heterogeneity, and (2) carcinogen-induced high mutational burden appears to correlate with the response to checkpoint inhibitors (McGranahan et al., 2016). Indeed, the FDA recently approved programmed cell death 1 (PD-1) checkpoint inhibitors for treatment of metastatic NSCLC (Brahmer et al., 2015; Mok and Loong, 2016). However, the immune system acts dynamically, often in localized tumor sub-regions such as tertiary lymphoid structures (TLSs) (Leslie, 2016), and reliable prognostic biomarkers for immunotherapy are lacking (Mok and Loong, 2016). Given this, genetically engineered mouse models (GEMMs) could serve to identify key mechanisms in which the immune microenvironment regulates tumor progression. As an example, depletion of TLS-associated regulatory T cells recently was shown to restore anti-tumor T cell responses in an NSCLC model driven by oncogenic *Kras* and loss of *Trp53* (*p53*) (Joshi et al., 2015).

Various NSCLC GEMMs, utilizing either conditional genetic or viral induction, have been used to address the relative contributions of genetic drivers and cells of origin to the generation of histopathological diversity and proliferative phenotypes (Leeman et al., 2014). Specifically, expression of oncogenic *Kras*, with or without additional loss of the *p53* tumor suppressor, drives transformation of $CC10^+$ cells in the BADJs at the terminal bronchioles, possibly involving dual $CC10^+/SPC^+$ cells, as well as of SPC^+ AT2 cells (Kim et al., 2005; Sutherland et al., 2014; Xu et al., 2012). Interestingly, $CC10^+$ and SPC^+ progenitors appear to distinctly contribute to AC tumorigenesis, evidenced by differential *Kras*- or *Kras*;*p53*-induced histopathology spectra (Lin et al., 2012; Sutherland et al., 2014). In addition, $Kras^{G12V}$ yields malignant AC mostly from SPC^+ progenitors, whereas $CC10^+$ cells develop more benign lesions requiring an adenoviral inflammatory response (Mainardi et al., 2014). Thus, $CC10^+$ club cells appear to show partial resistance to malignant transformation by oncogenic *Kras*, possibly due to differential Notch activity (Xu et al., 2014b).

While progenitor-specific etiologies of lung ACs are well described, these are less clear for ASC and SCC histotypes. Airway basal cells have been proposed to act as SCC progenitors following the loss of *Pten* with *Tgfbr2* or *Lkb1* (Malkoski et al., 2014; Xu et al., 2014a). Recent studies have further shown that AC derived from SPC^+ cells can transdifferentiate into SCCs via an intermediate ASC stage (Han et al., 2014; Li et al., 2015). Among NSCLC GEMMs, *Kras*;*Lkb1* mice infected with Ad5-CMV-Cre produce the full spectrum of histotypes, namely, AC, SCC, ASC, and large cell carcinomas (Ji et al., 2007). This prompted us to employ $CC10^+$ and SPC^+ progenitor cell-restricted adeno-Cre viruses, previously used to identify cells of origin in lung cancer GEMMs (Sutherland et al., 2011), to dissect progenitor cell roles in establishing NSCLC phenotypic and microenvironmental heterogeneity in conditional *Kras*;*Lkb1* mice. Our results show that $CC10^+$ and SPC^+ progenitor cells differentially contribute to histotype diversity and that $CC10^+$ cell-derived lesions are more proliferative. Furthermore, we establish $CC10^+$ cells as the predominant progenitors of the ASC histotype, and we show that ASCs exhibit a histotype-specific immune microenvironment.

RESULTS

Cell of Origin Defines Survival of Mice following Oncogenic *Kras* Expression and Loss of *Lkb1*

To investigate the relative contribution of lung progenitors in determining disease progression and histopathology in the *Kras*;*Lkb1* GEMM, mice were infected intranasally with 1×10^7 plaque-forming units (PFUs) or 2.5×10^9 PFUs of Ad5-CC10-Cre virus or Ad5-SPC-Cre virus, respectively. Since distal airway-located SPC^+ AT2 cells are not targeted as readily, titers were set based on their ability to achieve comparable infection rates using *mT/mG* Cre-reporter mice (Muzumdar et al., 2007). Similar to previous data (Sutherland et al., 2014), Ad5-CC10-Cre primarily targeted bronchiolar walls and BADJ areas, while alveolar cells were targeted primarily by Ad5-SPC-Cre (Figure S1A). Lungs from *Kras*;*Lkb1*;$Rosa26^{mT/mG}$ Cre-reporter mice were examined at 3–4 weeks post-infection, and accurate bronchiolar ($CC10^+$ cells) or alveolar (SPC^+ cells) membrane GFP labeling was confirmed by anti-CC10 and anti-SPC or immunohistochemistry (IHC), respectively; with these viral titers, we showed that ~0.8% of the total number of lung cells were targeted by Ad5-CC10-Cre or Ad5-SPC-Cre viruses (Figure S1B). We next followed cohorts of infected mice for late-stage tumor formation and euthanized mice when moribund. All lesions induced following Ad5-CC10-Cre and Ad5-SPC-Cre infection showed loss of LKB1 protein expression, confirming dual gene recombination (Figure S1C; Table S1). Kaplan-Meier survival analysis showed that mice infected with Ad5-CC10-Cre had a significantly shorter latency compared with Ad5-SPC-Cre (median survival 79 versus 120 days; Figure 1A), suggesting that tumors initiated from $CC10^+$ progenitor cells developed faster and/or more aggressive lung disease.

Cell of Origin Defines the *Kras*;*Lkb1*-Driven Histopathology Spectrum

Next, histopathological analyses of lesions formed in the full set of lung lobes from moribund Ad5-CC10-Cre- or Ad5-SPC-Cre-infected *Kras*;*Lkb1* mice were performed. We hereto adhered to the International Association for the Study of Lung Cancer/American Thoracic Society/European Respiratory Society (IASLC/ATS/ERS) NSCLC classification system (Travis et al., 2011), guided by an expert lung pathologist (Figure 1B). Two major histotypes were detected, namely, (1) ASCs, which contained an inner AC core expressing the AC biomarker NKX2-1 surrounded by an outer squamous region co-expressing both the squamous biomarker p63 and NKX2-1, and (2) ACs with invasive characteristics conferring loss of the alveolar structure. ASCs were predominantly detected in the Ad5-CC10-Cre cohort (5/5 mice, 20/60 lesions total) compared to the Ad5-SPC-Cre cohort (1/5 mice, 3/171 lesions total) (Figures 1C and S1D; Table S1). In line with a previous study, all ASCs expressed the squamous cell marker cytokeratin 5 (KRT5), but no staining for the nuclear SOX2 SCC marker was detected (Mukhopadhyay et al., 2014) (Figure S1E). In contrast, ASCs in the *Pten*;*Smad4* GEMM were reported to express SOX2 (Liu et al., 2015), suggesting that its expression in ASC could be dependent on driver genotype. To investigate SOX2 expression in human ASCs, we analyzed a tissue microarray (TMA)

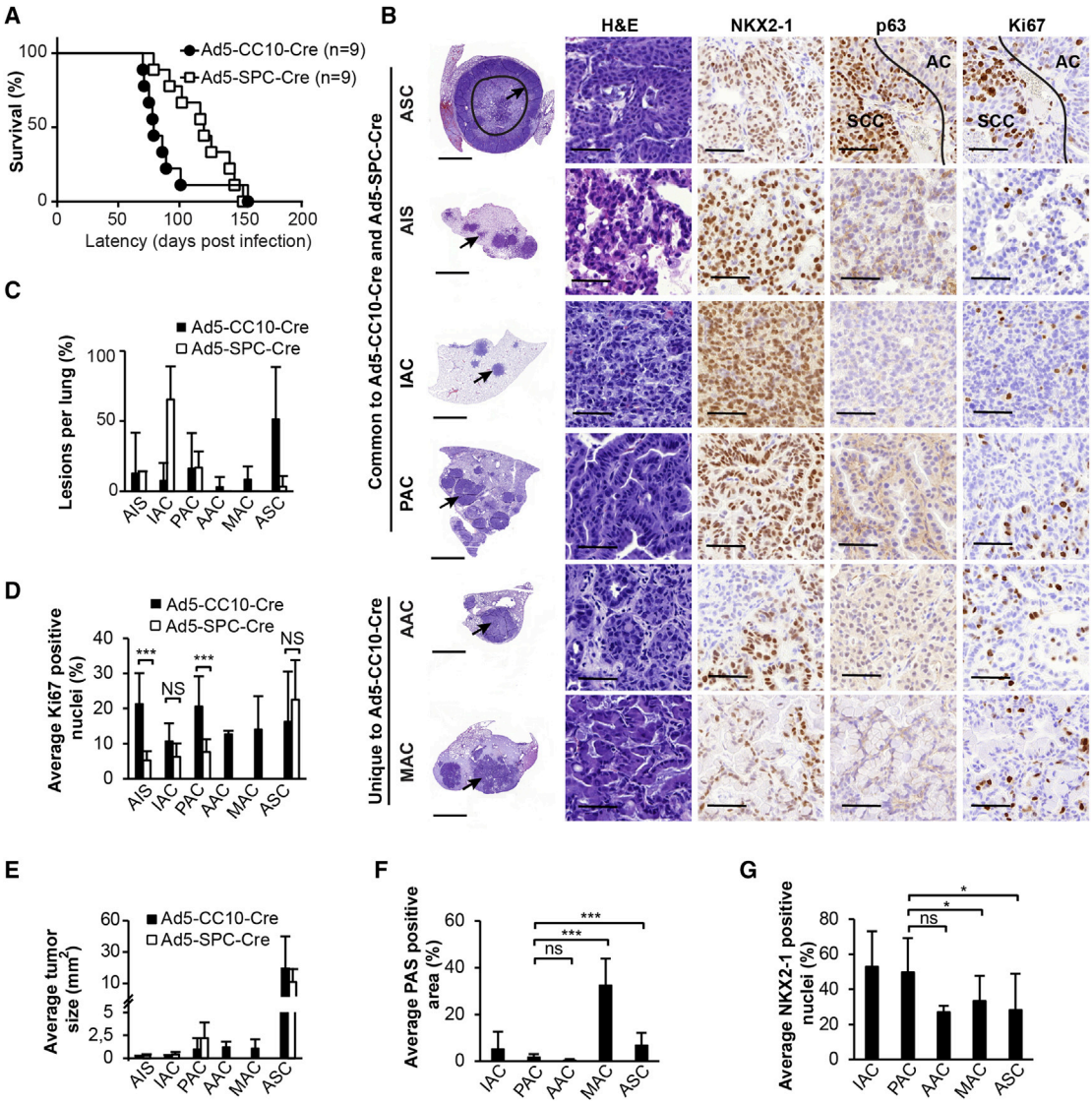

Figure 1. Cell of Origin Defines the Histopathology Spectrum and Associated Survival Differences of *Kras*;*Lkb1*-Driven Lung Tumors

(A) Kaplan-Meier survival curves of *Kras*;*Lkb1* mice show median survival of 79 days for Ad5-CC10-Cre (1×10^7 PFUs, black symbols) versus 120 days for Ad5-SPC-Cre infections (2.5×10^9 PFUs, white symbols). Significance value, p = 0.0125 with a Gehan-Breslow-Wilcoxon test.

(B) Histopathology analysis for tumors harvested from moribund Ad5-CC10-Cre and Ad5-SPC-Cre mice. Arrows indicate areas depicted in higher magnification IHC analyses with the indicated antibodies; the solid line separates SCC and AC regions of ASC.

(C) Quantification of histopathology-specific lesions, from n = 5 animals per virus, shows ASC as the predominant histopathology for Ad5-CC10-Cre- and IAC for Ad5-SPC-Cre-treated mice (see also Figure S1C).

(D) Histopathology-specific quantification of Ki67-positive nuclei is shown (see also Figure S2A).

(E) Lesion size quantification of animals analyzed in (C) shows that ASC tumors are the largest lesions.

(F) Quantification of PAS-positive tumor areas for lung lesions infected with Ad5-CC10-Cre virus (n = 4) is shown (see also Figure S2C).

(G) Quantification of NKX2-1-positive nuclei on samples analyzed in (F). Error bars represent mean ± SD. Student's t test p values, *p < 0.05 and ***p < 0.001. Scale bars, 2,000 μM for lung lobes and 50 μM for magnified images. AIS, adenocarcinoma in situ; IAC, invasive AC; PAC, papillary AC; AAC, acinar AC; MAC, mucinous AC; ASC, adenosquamous carcinoma.

containing clinical ASC samples. SOX2 expression was detected in 8/12 samples and was predominantly limited to the SCC component. Also, 7/12 ASC samples were LKB1 negative, including 2/4 SOX2-negative specimens (Figure S1F; Table S1), suggesting that ASCs from *Kras*;*Lkb1* GEMMs may represent a distinct subset of human ASC.

Both Ad5-CC10-Cre and Ad5-SPC-Cre induced invasive ACs (IACs), comprised of well or moderately differentiated lesions, and IACs were accompanied by pre-invasive adenocarcinoma in situ (AIS) (Figures 1B and 1C; Table S1). Deeper analysis of moderately differentiated IACs based on growth pattern revealed a spectrum of three AC subtypes, namely, pure mucinous

AC (MAC), papillary AC (PAC), and acinar AC (AAC). Tumors with a lepidic growth pattern at the lesion border but otherwise invasive were considered IAC (Figure S1G). Of these five AC lesion types, pure MACs and AACs were detected following Ad5-CC10-Cre infection (Figures 1B and 1C). Positivity for the AC biomarker NKX2-1, a differentiation marker frequently lost during invasive progression, was highest in IACs with or without papillary growth, whereas MACs and AACs induced by Ad5-CC10-Cre showed less NKX2-1-positive cells (Figure 1B). The majority of IAC subtypes were negative for p63 (Figure 1B), although one Ad5-CC10-Cre-induced PAC and a small proportion of MACs showed sporadic p63 staining (Figure S1H). The latter resembles clinical ACs, where 30% of lesions show p63 expression, yet are classified as AC based on morphological features (Au et al., 2004).

Inspection of *Kras*;*Lkb1* lesions during early-stage tumorigenesis showed that both viruses induced detectable lesions at 6 weeks post-infection (Figure S1I). At this stage, Ad5-CC10-Cre induced NKX2-1-positive luminal papillary hyperplasias of epithelial cells in the terminal bronchioles, with sparse staining for p63. Ad5-SPC-Cre-induced lesions at 6 weeks were NKX2-1-positive pre-invasive AIS located in the alveoli. At 9 weeks post-infection, Ad5-CC10-Cre lesions consisted of AIS, IAC, PAC, MAC, and ASC, similar to the histopathology types detected in moribund mice. At this time point, we observed SCC in one of four mice (Figure S1I), while no SCC was seen at later stages. Lesions at 9 weeks following Ad5-SPC-Cre infections were IACs or PACs and lacked squamous features altogether. Taken together, expression of oncogenic *Kras* with *Lkb1* loss elicited a progenitor cell-specific difference in histopathology spectrum formation. $CC10^+$ cell-derived lesions showed a wider spectrum of AC histotypes, including pure mucinous and acinar AC, and they were predominantly of the adenosquamous histotype, while SPC^+ cell-derived tumors were primarily ACs. This suggests a possible lung airway epithelium-restricted role for LKB1 in the normal lung, potentially explaining the different effects of *Lkb1* deletion in $CC10^+$ and SPC^+ epithelial progenitors.

Cell of Origin and Histotype-Specific Differences in Tumor Proliferation and Differentiation Status

To investigate histotype-specific proliferation rates, percentages of Ki67-positive nuclei across all lesions were quantified at the end stage. This analysis showed that some of the Ad5-CC10-Cre-induced tumor types, in particular Ad5-CC10-Cre-induced AIS lesions and PACs, exhibited higher proliferation rates compared with Ad5-SPC-Cre-derived lesions (Figures 1D and S2A). Contrary to this trend, there was no difference in proliferation detected in ASCs induced by Ad5-CC10-Cre or Ad5-SPC-Cre infection. The SCC region of ASCs exhibited higher proliferation than the AC regions (Figure 1B), with the greater proliferative capacity of the SCC histotype appearing to influence rapid proliferation of ASCs independent of their cell of origin. We further analyzed expression of the high mobility group AT-hook 2 (HMGA2) transcription factor commonly expressed in more poorly differentiated and invasive tumors (Snyder et al., 2013; Sutherland et al., 2014; Winslow et al., 2011). Homogeneous expression of HMGA2 in ASCs was seen, whereas all other histopathologies had negative to sparse expression (Figure S2B). Furthermore, macroscopically all ASCs were much bigger in size, ranging from 20 to 30 mm^2 compared to smaller than 3 mm^2 lesions for all other histotypes (Figure 1E). The shorter survival of Ad5-CC10-Cre-infected mice thus correlated with an increased propensity for highly proliferative PAC and AIS lesions and large ASC tumors.

Since the molecular basis and etiology of AC subtypes is thus far unknown, we decided to more deeply study the mucinous ACs, a subtype of human lung cancer here detected upon Ad5-CC10-Cre infection. Mucin production was confirmed with periodic acid Schiff's (PAS) staining (Figure S2C). Consistent with the finding that haploinsufficiency of NKX2-1 cooperates with $Kras^{G12D}$ in MAC progression (Maeda et al., 2012; Snyder et al., 2013), we further observed reduced expression of NKX2-1 in PAS-positive mucinous tumors compared to well-differentiated PACs (Figures 1F, 1G, S2D, and S2E). PAS positivity also was detected in the AC regions of ASCs, bronchiolar luminal papillary hyperplasias, and in some of the IACs (Figures S2C and S2F). This suggests that progression to MAC may involve bronchiolar luminal papillary hyperplasias or IAC as an intermediate state. Taken together, these results show that $CC10^+$ progenitor cells have the ability to give rise to advanced AC with mucinous differentiation and have a clear influence on histotype spectrum, tumor proliferation, and differentiation status.

Kras;*Lkb1* Tumors Show Histotype-Specific Gene Expression Signatures

To gain insights into histotype-specific molecular heterogeneities, we compared RNA expression profiles of Ad5-CC10-Cre-derived ASCs and Ad5-SPC-Cre-derived PACs, representing the predominant progenitor-specific *Kras*;*Lkb1* histotypes at the end stage of disease progression (Figure S3A). Tumor histopathology was confirmed by the expression of p63 protein specifically in ASCs (Figure S3B). Unsupervised hierarchical clustering using adjusted p value < 0.01 LogFC > 1 as a cutoff revealed 340 differentially expressed genes showing distinct clustering of ASC and PAC tumors (Figure 2A). We next asked how these gene signatures related to previously published histotype-specific gene signatures. Since no human ASC gene signatures are available, we instead utilized SCC versus AC comparative gene expression data. These were comprised of a recently described comparison of SCC elicited by conditional *Lkb1* and *Pten* loss to $Kras^{G12D/+}$-derived AC tumors (Xu et al., 2014a) and a human SCC versus AC comparative gene expression study (Kuner et al., 2009). Using a cutoff value of $p < 0.01$ LogFC > 1, we identified 29 and 11 commonly upregulated or downregulated genes, respectively (Figure 2B; Table S2). SCC-enriched genes encompassed known human SCC biomarkers transformation-related protein 63 (*Trp63*) and multiple basal cytokeratins (Krt) (Figure 2C). Interestingly, the recently described AC biomarker napsin A (*Napsa*), a pepsin family aspartic proteinase (Turner et al., 2012), also was found enriched in the murine PACs.

We further compared our dataset to untransformed murine airway basal cell expression profiles to determine if basal or epithelial signatures contribute to ASC (Rock et al., 2009). This identified 108 genes commonly enriched in Ad5-CC10-Cre-derived ASC and airway basal cells (Figure S3C; Table S2). In

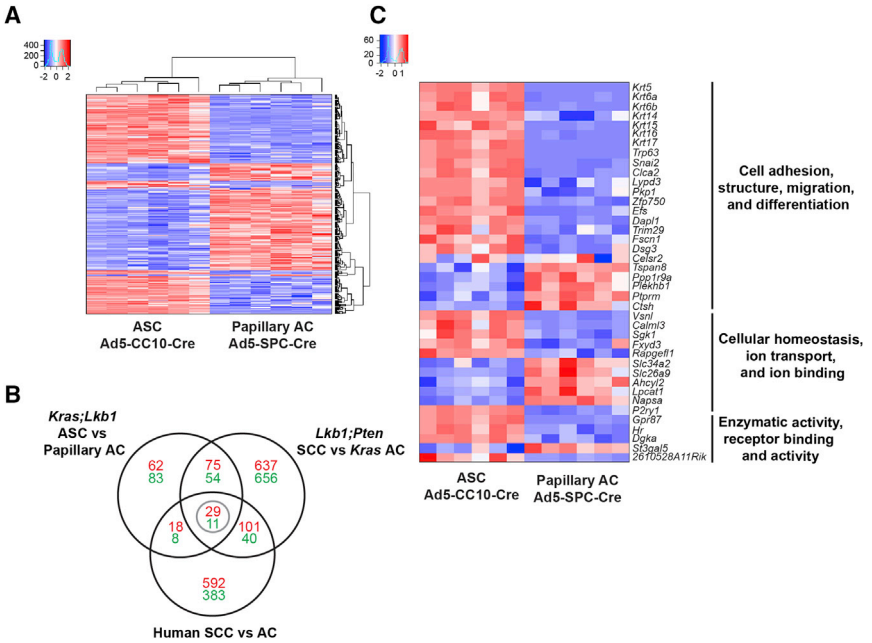

Figure 2. Comparative Gene Expression Analysis Indicates Squamous Expression Profile in Ad5-CC10-Cre-Derived ASC Tumors

(A) Unsupervised hierarchical clustering of Ad5-CC10-Cre-derived ASC and Ad5-SPC-Cre-derived PAC tumors, with $p < 0.01$ LogFC > 1 as a cutoff, shows distinct histopathology-specific gene expression signatures.

(B) Venn diagram illustrating comparative expression analyses of gene set used in (A), *Lkb1*;*Pten* SCC versus *Kras* AC (Xu et al., 2014a; GSE54353), and human SCC versus AC tumors (Kuner et al., 2009, GSE10245). Upregulated and downregulated genes are in red and green fonts, respectively.

(C) Common up- and downregulated genes of datasets shown in (B) represented as a heatmap of gene expression values from *Kras*;*Lkb1* ASC versus PAC datasets. Insets in (A) and (C) show the distribution of samples within scaled expression values.

addition to known stratified squamous epithelial marker genes *Trp63*, basonuclin 1 (*Bnc1*), stratifin (*Sfn*), and cytokeratins, we found common enrichment of pro-inflammatory cytokine interleukin 1 beta (*Il1b*) and its interleukin-1 receptor, type II (*Il1r2*). As expected, the AC biomarker SPC was commonly downregulated in airway basal cells and ASC. Finally, our dataset was compared with published ASC gene expression signatures from the *Kras*;*Lkb1* GEMMs (Ji et al., 2007), showing 23 commonly enriched genes (Figure S3C; Table S2), including SCC signature genes such as *Trp63* and cytokeratins. Collectively, our results show that, even though $CC10^+$ lung progenitor cell-derived ASCs display features of AC at the histological level, they exhibit SCC histotype-specific gene signatures.

Kras;*Lkb1* and *Kras*;*p53* Tumors Show Histotype-Specific Expression of Immune-Related Genes

A recent study showed that Ad5-CMV-Cre-derived *Kras*;*Lkb1* tumors maintain an immunosuppressive microenvironment through the recruitment of tumor-associated neutrophils (TANs) and production of pro-inflammatory cytokines to suppress cytotoxic T cells (Koyama et al., 2016). As our results demonstrate that the cell of origin influences the histotype spectrum in the *Kras*;*Lkb1* GEMM, we investigated if the immunosuppressive phenotype of this model is restricted to a particular tumor histotype. Interestingly, analysis of *Kras*;*Lkb1* Ad5-CC10-Cre ASC and Ad5-SPC-Cre PAC gene signatures by ingenuity pathway analysis (IPA) revealed granulocyte adhesion and diapedesis and antigen presentation as the top most altered canonical pathways, implying histotype-specific differences in immune-related functions (Figure 3A).

To assess if the tumor genotype has an effect on the immune gene signatures, we compared RNA expression profiles of *Kras*;*p53* PACs to *Kras*;*Lkb1* ASC and PAC profiles, which confirmed that selected cytokine, chemokine, and antigen presentation pathway genes showed histopathology-dependent and genotype-independent expression differences (Figure 3B). Specifically, ASCs showed enrichment of pro-inflammatory genes related to neutrophil infiltration, namely, the cytokine *Il1b* and S100 calcium-binding proteins A8 and A9 (*S100a8* and *S100a9*), as well as the enzyme arginase, liver (*Arg*1), a key mediator of immunosuppression (Munder et al., 2006; Ryckman et al., 2003). Furthermore, ASCs showed downregulation of both class I (*H2-M2* and *H2-D1*) and class II (*H2-DMa*, *H2-Ab1*, and *H2-DMb1*) major histocompatibility complex (MHC) genes. Conversely, the lymphocyte and monocyte chemoattractants, chemokine *Ccl17* and *Ccl6*, and the lung-specific chemokine *Cxcl15* were expressed in PACs. Quantitative real-time PCR analysis on a selected set of genes confirmed increased *Il1b* and *Arg1* and decreased MHC class I expression specifically in *Kras*;*Lkb1* ASCs, and it confirmed variable expression of MHC class I genes in *Kras*;*p53* PACs (Figure 3C). Finally, to assess whether the cell of origin influences expression of immune-related genes, we included in the qPCR validation panel a Ad5-CC10-Cre-derived PAC and two rare Ad5-SPC-Cre-derived *Kras*;*Lkb1* ASCs. This confirmed that also the ASCs derived from SPC^+ progenitors show increased *Il1b* and *Arg1* and decreased MHC expression (Figure S3D). In summary, our data indicate histopathology-dependent but oncogenotype-independent expression of immune-related genes. Particularly, ASCs arising in *Kras*;*Lkb1* mice exhibit an immune gene signature favorable for neutrophil infiltration and escape from tumor antigen presentation by downregulation of antigen presentation molecules.

Kras;*Lkb1* ASCs Show Histotype-Specific Recruitment of $CD11b^+$ $Gr\text{-}1^+$ TANs

It has been shown that $CD11b^+$ $Ly\text{-}6G^+$ TANs are the major immune cell population in *Kras*;*Lkb1* compared to *Kras* lung tumors

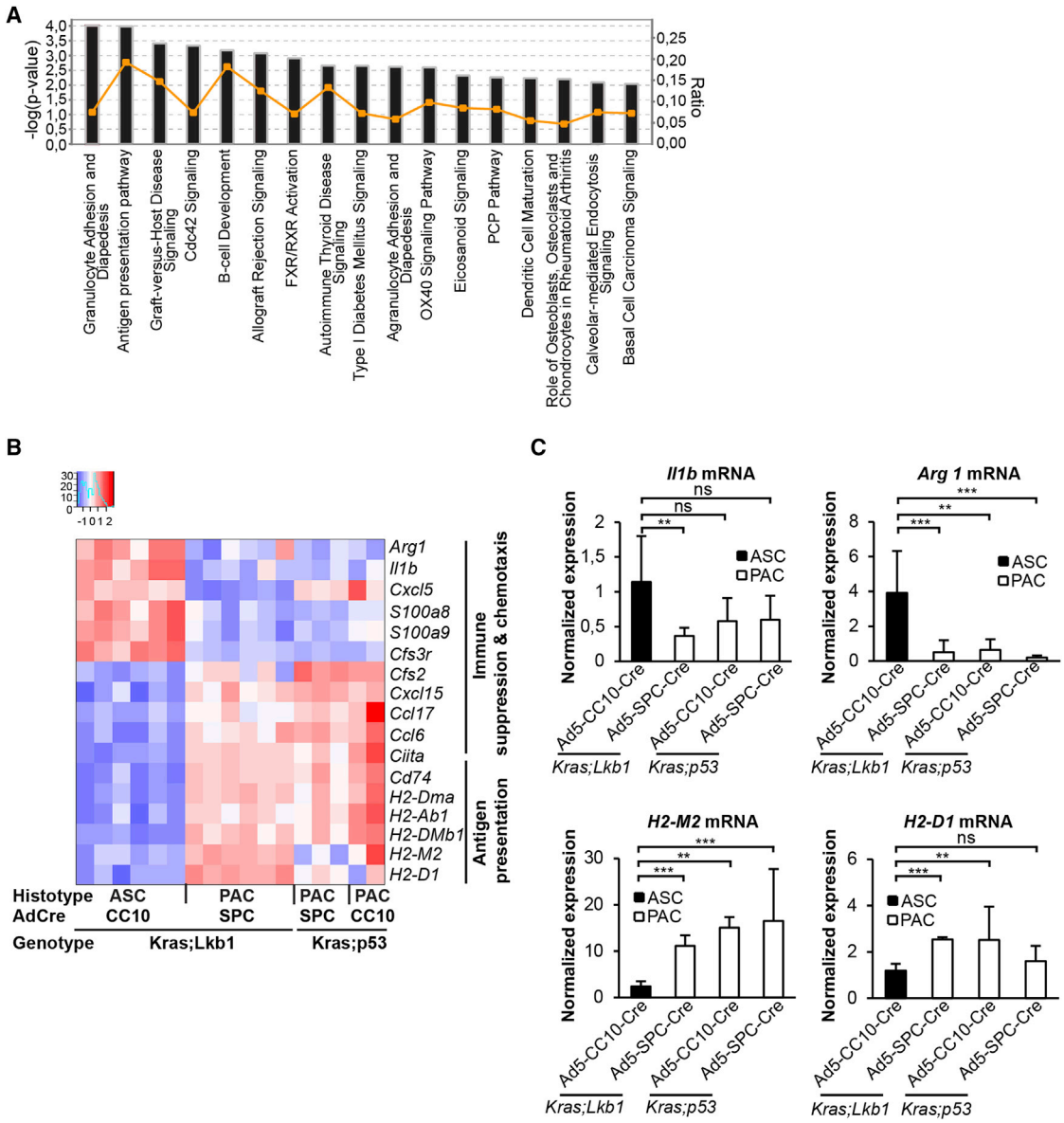

Figure 3. Distinct Immune-Related Gene Expression Signatures Suggest ASC versus PAC Histopathology-Specific Tumor Immune Microenvironments

(A) IPA canonical pathway analysis shows enrichment of several immune-related genes in *Kras*;*Lkb1* Ad5-CC10-Cre-derived ASCs compared with Ad5-SPC-Cre-derived PACs. A −log (p value) greater than 2 was used as a cutoff.

(B) Heatmap representing immune-related genes differentially expressed in *Kras*;*Lkb1* Ad5-CC10-Cre-derived ASC and Ad5-SPC-Cre-derived PAC and *Kras*;*p53* Ad5-CC10-Cre-derived and Ad5-SPC-Cre-derived PAC tumors with $p < 0.01$ LogFC > 1 as a cutoff. The inset shows the distribution of samples within scaled expression values.

(C) qPCR validation of *Il-1β*, *Arg1*, *H2-M2*, and *H2-D1* gene expression in ASC (n = 13 tumors) and PAC (PAC, n = 8 tumors) from *Kras*;*Lkb1* and Ad5-CC10-Cre-derived (n = 4 tumors) and Ad5-SPC-Cre-derived (n = 7 tumors) PACs from *Kras*;*p53* genotypes. Gene expression was normalized against the housekeeping *Rpl19* mRNA. Error bars represent mean ± SD. Student's t test p values, $^{**}p < 0.01$ and $^{***}p < 0.001$.

(Koyama et al., 2016). Since we observed histotype-dependent immune gene signatures, we more deeply investigated the immune cell compositions in the predominant *Kras*;*Lkb1* ASC and PAC histotype lesions. Tumor tissue-expressed interleukin-1β (encoded by *Il1b*) has been shown to activate and mobilize TANs, which mediate immunosuppression among others by expression of arginase 1, an enzyme responsible for the depletion of extracellular L-arginine required for T cell proliferation (Raber et al., 2012; Tu et al., 2008). The gene expression analysis revealed ASC-specific expression of neutrophil chemoattractant *Il1b*, and T cell-suppressive enzyme *Arg1*, suggesting that TAN infiltration in the *Kras*;*Lkb1* model could be ASC

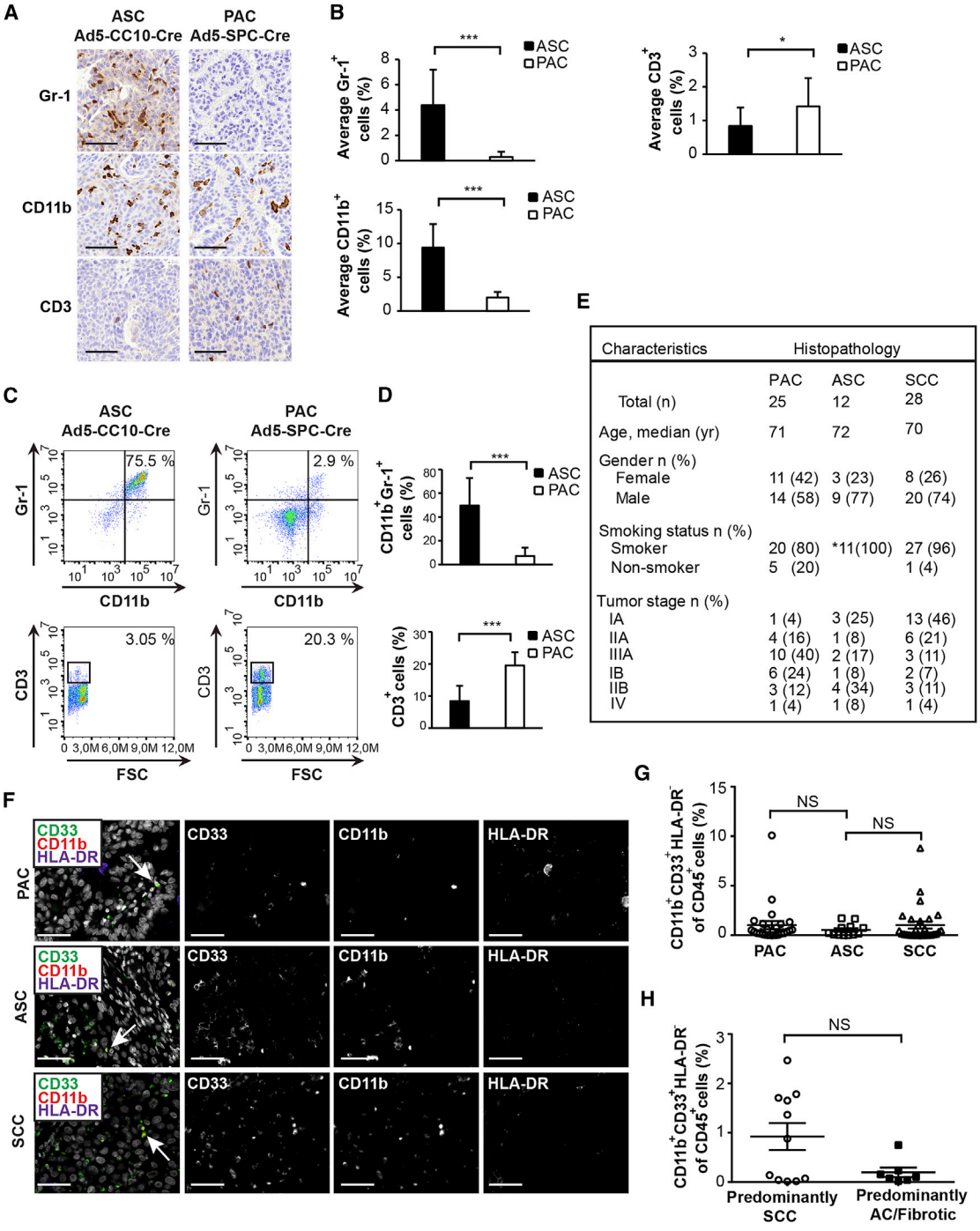

Figure 4. Histotype-Specific Immune Cell Profiling of Mouse and Human Lung Tumors

(A) Representative IHC for Gr-1, CD11b, and CD3 in *Kras*;*Lkb1* Ad5-CC10-Cre-derived ASC and Ad5-SPC-Cre-derived PAC is shown. Scale bar, 50 μm.

(B) Quantification of IHC for Gr-1, CD11b, and CD3 (n = 5 mice) showing higher intratumoral infiltration of Gr-1- and CD11b-positive cells and lower intratumoral infiltration of CD3-positive T cells in *Kras*;*Lkb1* Ad5-CC10-Cre-derived ASCs compared to Ad5-SPC-Cre-derived PACs. Error bars represent mean ± SD. Student's t test p values, *$p < 0.5$ and ***$p < 0.001$.

(C) Representative flow cytometry scatterplots showing CD11b and Gr-1 double-positive myeloid cells and CD3-positive T cells in Ad5-CC10-Cre-derived ASC and Ad5-SPC-Cre-derived PAC from *Kras*;*Lkb1* mice. Plots are gated for live, single, and $CD45^+$ cells.

(D) Flow cytometry analysis of $CD11b^+$ $Gr\text{-}1^+$ cells and $CD3^+$ T cells, represented as the percentage of total $CD45^+$ cells, shows higher $CD11b^+$ $Gr\text{-}1^+$ and reduced amounts of $CD3^+$ T cells in *Kras*;*Lkb1* Ad5-CC10-Cre-derived ASCs (n = 9, three mice) compared to Ad5-SPC-Cre-derived PACs (n = 9, three mice). Error bars represent mean ± SD. Student's t test p values, *$p < 0.05$ and ***$p < 0.001$.

(legend continued on next page)

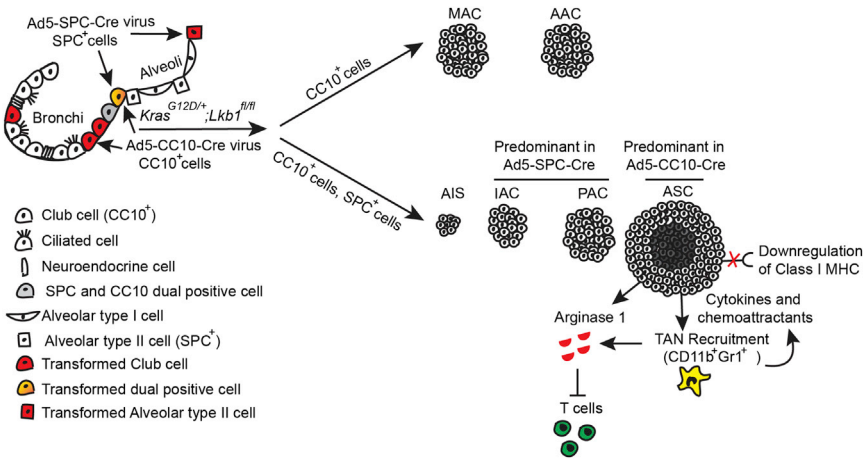

Figure 5. ASC Histotype-Specific Recruitment of CD11b$^+$ Gr-1$^+$ TANs

Schematic representation summarizing lung progenitor cell-specific lesion etiology following the expression of oncogenic *Kras* concomitant with the loss of *Lkb1* in CC10$^+$ or SPC$^+$ cells. Both CC10$^+$ and SPC$^+$ progenitors can give rise to IAC, AIS, PAC, and ASC, with ASC most prevalent for CC10$^+$ cells. CC10$^+$ cells give rise to pure MAC and AAC. ASCs exhibit a distinct immune microenvironment specified by TAN infiltration and increased arginase 1 to suppress T cell proliferation and survival in the tumor microenvironment.

histotype specific. We next studied histotype-specific immune cell infiltration by immunostaining. Immunohistochemical analysis revealed enrichment of intra-tumoral CD11b$^+$ and Gr-1$^+$ cells, concomitant with a reduced number of intra-tumoral CD3$^+$ T cells, specifically in ASCs compared to PACs (Figures 4A, 4B, and S3E). Murine TANs consist of CD11b$^+$ Ly-6G^{hi} Ly-6C^{low} granulocytic and CD11b$^+$ Ly-6G^{low} Ly-6C^{hi} monocytic populations (Talmadge and Gabrilovich, 2013). Flow cytometry analysis confirmed a higher percentage of CD11b$^+$ Gr-1$^+$ and CD11b$^+$ Ly-6C^{low} TANs and a lower percentage of CD3$^+$ T cells in the CD45$^+$ leukocyte population in ASC tumors (Figures 4C, 4D, S3F, and S3G). Due to the high variability of CD4$^+$- and CD8$^+$ T cell infiltration in the PAC tumors, no statistically significant difference in the percentage of CD4$^+$ or CD8$^+$ T cells was detected between ASCs and PACs (Figures S3F and S3G). Interestingly, although spleen-derived TANs have been shown to promote tumorigenesis of *Kras*;*p53* ACs (Cortez-Retamozo et al., 2012), our *Kras*;*p53* tumor analysis showed low yet highly variable amounts of CD11b$^+$ Gr-1$^+$ cells (Figures S4A and S4B), suggesting that TAN infiltration in this model could be dependent on tumor differentiation status.

To study if the identified *Kras*;*Lkb1* tumor histotype-specific immune microenvironment is detected in human NSCLC, we constructed patient tumor TMAs containing 12 ASCs, 25 PACs, and 28 SCCs (Figures 4E and S4C). Quantification of immunohistochemical co-staining for the human TAN markers CD11b, CD33, and HLA-DR did not show a statistically significant difference in CD11b$^+$ CD33$^+$ HLA-DR$^-$ TANs between histopathology groups (Figures 4F, 4G and S4D), although numbers of TANs were slightly higher in SCCs. We did, however, detect a trend in increased numbers of CD11b$^+$CD33$^+$HLA-DR$^-$ cells in spots representing the squamous component of the ASC tumors (Figures 4H and S4E). We further found that, while 7/12 patient-derived ASC tumors were negative for LKB1, no increased TAN infiltration was detected in these samples (Figures S4F and S4G). Taken together, we provide evidence that *Kras*;*Lkb1* ASC tumors exhibit an apparent immunosuppressive microenvironment manifested by intratumoral TANs and, importantly, this appears to be a histotype-specific phenomenon.

DISCUSSION

The relative roles of progenitor cells and their respective niches in establishing potential histotype-specific tumor microenvironments remain poorly understood. We show here that CC10$^+$ and SPC$^+$ progenitor cells differentially contribute to histotype diversity in the *Kras*;*Lkb1* GEMM, with CC10$^+$ cells serving as the predominant progenitor of the ASC histotype. While the exact identity of the cell of origin(s) giving rise to ASCs remains unknown, our data clearly indicate that its progenitor is enriched in the population of cells targeted by the Ad5-CC10-Cre virus. Furthermore, we show that the CC10$^+$-derived tumors are generally more proliferative and that ASCs are enriched for TANs (Figure 5). Interestingly, similar to our observations, human ASCs often contain PAS-positive AC regions (Kanazawa et al., 2000), indicating a precise recapitulation of human ASC pathology in the *Kras*;*Lkb1* model.

Clinically, AC is the most common lung cancer subtype, further sub-classified as pre-invasive, minimally invasive, and invasive AC (Travis et al., 2011). We here find that *Kras*;*Lkb1* progenitors have a capacity to generate three subtypes of invasive AC, namely papillary, acinar, and mucinous AC, thus closely resembling the mixed histotype spectrum typical of human disease. Importantly, MACs and AACs are exclusively initiated

(E) Clinical and demographic characteristics of NSCLC patients used in the TMA analysis (*11/12 ASC patients were smokers, and the smoking status of one ASC patient was unknown). Staging of the tumors was performed according to the World Health Organization (WHO) book 2015.
(F) Representative immunohistochemical staining for CD33, CD11b, and HLA-DR in human PAC, ASC, and SCC tumor samples is shown. Scale bar, 50 μm.
(G) Quantification of immunostainings for CD11b-, CD33-positive, and HLA-DR-negative cells in human PAC (n = 25), ASC (n = 12), and SCC (28). The amount of CD11b and CD33 double-positive and HLA-DR-negative myeloid cells is normalized against the number of chromogenic CD45$^+$ cells (see also Figure S4D).
(H) Quantification of immunostainings for CD11b-, CD33-positive, and HLA-DR-negative cells in ASC TMA spots categorized by the predominance of SCC, AC, and fibrotic regions (see also Figure S4E). Error bars represent mean ± SEM. Nonparametric Kolmogorov-Smirnov test shows no statistical difference between the tumor histopathology groups.

from CC10$^+$ progenitors, implying niche/stem cell-dependent contributions to histotype diversity. The phenotypic diversity of CC10$^+$ progenitor-derived tumors could be explained by the targeting of multiple functionally distinct, albeit CC10-expressing progenitors residing in distinct compartments of the lung (Rawlins et al., 2009; Zheng et al., 2014). Such potential progenitors include airway goblet cells co-expressing mucin and CC10, located near the terminal bronchioles (Boers et al., 1999), as we observe many PAS-positive cells in early bronchiolar luminal papillary hyperplasias. MACs may thus arise from secretory cells that confer dual goblet and club cell features. Importantly, our study addresses the cell of origin-specific histotype diversity in the *Kras*;*Lkb1* GEMM, revealing a previously underappreciated capacity to model human NSCLC, where *LKB1* mutation is enriched across the spectrum of AC (13%) and ASC (22%), but not SCC (5%), lesions (Koivunen et al., 2008). This therefore warrants deeper dissection of the precise mechanisms in which progenitor subtypes contribute to histopathology-specific tumor biologies, for example, by using bimodal promoters.

We show evidence for a clear propensity of bronchiolar CC10$^+$ progenitors to form adenosquamous lesions, with all Ad5-CC10-Cre-treated animals developing ASC, while the incidence of ASC lesions arising from SPC$^+$ progenitors was extremely low. These rare ASCs may transdifferentiate from PACs, as reported earlier (Li et al., 2015). Alternatively, the rarity of Ad5-SPC-Cre-driven ASCs can be explained by a low incidence of dual CC10$^+$/SPC$^+$ progenitors in the alveoli or bronchioalveolar duct junctions (Rawlins et al., 2009). Interestingly, we observed several small SCC lesions among the IAC and ASCs at 9 weeks following Ad5-CC10-Cre infection, whereas at later stages no pure SCC lesions were detected. This stands in stark contrast to a previous study describing transdifferentiation of AC lesions to SCC via an intermediate ASC stage in the identical *Kras*;*Lkb1* GEMM (Han et al., 2014). One factor contributing to these differences could be the appreciated influence of mouse genetic background (Jiang et al., 2014) on tumor incidence and histotype spectrum formation. Future lineage-tracing studies could confirm whether ASCs transdifferentiate from a specific precursor histotype lesion and, further, which SPC$^+$ cell(s) act as the cell of origin for ASC.

Comparative gene expression analysis revealed that *Kras*;*Lkb1* ASCs show characteristics of murine and human SCCs. Furthermore, analysis of *Kras*;*Lkb1* and *Kras*;*p53* tumor histotype-specific expression profiles revealed differential immune-related gene signatures, which in *Kras*;*Lkb1* ASCs were associated with the recruitment of TANs and concomitant low T cell numbers, while papillary ACs expressed chemoattractants and showed higher yet variable T cell infiltration. Finally, ASCs may escape tumor antigen presentation and, hence, T cell-mediated toxicity by virtue of the detected decrease in class Ia/b MHC gene expression. Our results are corroborated by a recent study reporting *Lkb1* loss-dependent lung tumor immunosuppression, evidenced by increased TANs and reduced T cell numbers (Koyama et al., 2016). We here deepen the latter's finding by using cell-type-specific AdCre viruses to show that immunosuppression is specific to *Kras*;*Lkb1* ASCs and not ACs, uncovering histotype- rather than genotype-specific immune contextures. This data suggests that, in addition to genotype-specific stratification, an understanding of potential histotype-specific tumor microenvironments will be important in the clinical setting. Taken together, our data show that lung tumor pathogenesis is closely intertwined with immune modulation, and they emphasize a major contribution of the cell of origin in determining lesion-specific functional histopathology diversity.

Some ASC-specific immune modulatory features may be shared with SCC tumors, which showed a partial immune signature overlap (Table S2). Indeed, increased TAN infiltration has been reported also in SCCs of the *Lkb1*;*Pten* GEMM (Xu et al., 2014a). Outstanding questions are how such functional heterogeneity is tied with expression of the *Il1b* cytokine, already expressed at baseline in untransformed tracheal cells (Rock et al., 2009), and how our findings may relate to human disease. Interestingly, polymorphisms in *IL1B* have been associated with increased lung cancer risk, in particular SCC (Landvik et al., 2009). Furthermore, loss-of-function mutations in the HLA class I MHC gene have been reported for human lung SCC (Cancer Genome Atlas Research Network, 2012), indicating that immunosuppression may be a feature of human squamous lesions. However, no significant enrichment of TANs was observed in human patient ASC or SCC samples, possibly explained by the limited number of rare ASCs available for analysis, together with a high level of inter-sample variability and/or selective sampling of heterogeneous tumor sub-regions. In addition, clinical heterogeneity in co-occurring pathological conditions, such as COPD and prior glucocorticoid treatment, may affect immune cell infiltration. The finding that LKB1 expression status in human ASCs does not correlate with TAN infiltration is consistent with results from the *Kras*;*Lkb1* GEMM, where tumor genotype does not correlate with tumor immune microenvironment. Despite these limitations in achieving significant translational impact, our data support the utilization of tractable murine *Kras*;*Lkb1* GEMMs to study ASC pathology, and this model may serve to investigate immune-related tumor phenotypes also relevant to human disease. Improved translation of our findings to clinical disease requires the analysis of a greater number of human ASCs, as well as greater consideration of the impact of patients' other pathological conditions and prior clinical treatments on tumor immune properties. In addition, investigation of biomarkers and immunosuppressive markers beyond those described here will help to better understand the extent to which murine ASCs recapitulate human disease, and to investigate potential ASC-specific therapeutic targets.

In conclusion, our study provides important insights into the etiology of lung cancer histotype diversity, implying that the cell-of-origin biology and its physiological niche crucially define histopathology-specific tumorigenesis and formation of an immune microenvironment. Our data further suggest that the cell of origin crucially defines immune gene signatures, as *Kras*;*Lkb1* SPC$^+$ progenitors give rise to AC with immune features similar to *Kras*;*p53*. Such phenotypic dominance possibly relates to clinical evidence for clonal heterogeneity in the genetic makeup of tumor cells in histopathologically indistinct lesions (Heim et al., 2014). Future approaches will need to address which molecular aspects of CC10$^+$ and SPC$^+$ progenitors cooperate with *Kras*;*Lkb1* drivers to define histopathology diversity. It will be interesting to find out how this GEMM can be used for the

development of immune modulatory targets to achieve better control of ASC, an aggressive subtype of NSCLC (Nakagawa et al., 2003). While the progenitor cell-restricted *Kras*;*Lkb1* model has proved a robust tool to identify a distinct histotype-specific immunosuppressive microenvironment, the therapeutic potential of targeting the associated immune cell types to treat aggressive NSCLC has yet to be shown. While others have reported the efficacy of targeting the immunosuppressive microenvironment in *Kras*;*Lkb1* GEMMs (Koyama et al., 2016), the importance of the tumor histotype to therapeutic outcome was not addressed. The work presented here suggests that tumor histopathology will be a key determinant of response to these approaches. Therefore, future studies should elucidate the predicted histotype-dependent sensitivities to immunotherapeutic strategies, for example, by targeting pro-tumorigenic TAN functions or by re-priming the anti-tumor T cell response by class I MHC induction. Finally, our data underscore that the profiling of patient tumor histotype-specific functions and immune microenvironments should be taken into consideration together with stratified oncogenetic driver mutations.

EXPERIMENTAL PROCEDURES

Mouse Strain Information

Animal studies followed guidelines from the Finnish National Board of Animal Experimentation, and they were approved by the Experimental Animal Committee of the University of Helsinki and the State Provincial Office of Southern Finland (license number ESAVI-2010-04855/Ym-23). Mice harboring a conditional allele of mutant *Kras* (*Kras*LSL-$^{G12D/+}$; Jackson et al., 2001) or loss-of-function *Trp53* allele (*p53*$^{fl/fl}$; Marino et al., 2000) were purchased from The Jackson Laboratory. Conditional loss-of-function *Stk11*/*Lkb1* mice (*Lkb1*$^{fl/fl}$; Bardeesy et al., 2002) were received from Ron DePinho (MD Anderson). Further details are explained in the Supplemental Experimental Procedures.

Survival Analysis, Tissue Preparation, and Histopathology Analysis

Mice were sacrificed when showing symptoms of labored breathing and loss of weight. Kaplan-Meier survival curves were created with GraphPad Prism. Histopathology analysis was performed for whole-slide scans of H&E-stained paraffin sections. Details are explained in the Supplemental Experimental Procedures.

Immunohistochemistry

Immunistochemistry was performed on 4% formaldehyde-fixed and paraffin-embedded lungs using standard protocols. Quantitation of whole-slide scans acquired from PAS or immunohistological stained sections was performed using the Tissue Studio image analysis solution of the Definiens Developer XD 64 2.1 software. Details are explained in the Supplemental Experimental Procedures.

Microarray Gene Expression Profiling and qPCR Analysis

Total RNA from snap-frozen tumors was extracted using the NucleoSpin RNA II kit (MACHEREY-NAGEL). Expression profiling was done with Illumina Mouse WT-6 version 2 expression arrays. Microarray data are made available at GEO: GSE69552. The qPCR was performed for total mRNA extracted from snap-frozen tissue using iQ SYBR Green Supermix (Bio-Rad). Further details are explained in the Supplemental Experimental Procedures.

Comparative Gene Expression Analysis

Differentially expressed genes were compared to publicly available gene expression datasets made available via the NCBI GEO (http://www.ncbi.nlm.nih.gov/geo/) database. Details are explained in the Supplemental Experimental Procedures.

Flow Cytometry Analysis

Tumors were dissected from moribund mice and single-cell suspensions were incubated with rat anti-mouse antibodies. Detailed processing of the samples and antibody information can be found in the Supplemental Experimental Procedures.

Human Lung Cancer Samples and TMA

Archived formalin-fixed paraffin-embedded tumor specimens were collected from 65 NSCLC patients operated on during 2000–2015 at the Hospital District of Helsinki and Uusimaa (HUS) under an approval of the ethics committees of Joint Authority for the HUS. Based on the IASLC/ATS/ERS NSCLC classification system (Travis et al., 2011), 12 of the patients were diagnosed as adenosquamous carcinoma, 25 as papillary adenocarcinoma, and 28 as squamous cell carcinoma. Staging of human NSCLC histopathologies was performed by an expert lung pathologist. Details of the TMA construction are explained in the Supplemental Experimental Procedures.

Statistical Analysis

Gehan-Breslow-Wilcoxon test was used for the mouse survival curve analysis. Nonparametric Kolmogorov-Smirnov test was used to test statistical significance in the human patient immunohistochemistry-based immune cell quantitation. For the statistical analysis of the rest of the analyses, we used Student's t test (two-tailed and equal variance). A p value < 0.05 was considered significant. Error bars indicate SEM for human patient immune cell infiltrations and SD for the rest.

ACCESSION NUMBERS

The accession number for the microarray data reported in this article is GEO: GSE69552.

SUPPLEMENTAL INFORMATION

Supplemental Information includes Supplemental Experimental Procedures, four figures, and two tables and can be found with this article online at http://dx.doi.org/10.1016/j.celrep.2016.12.059.

AUTHOR CONTRIBUTIONS

E.W.V. conceived and supervised the study. A.S.N., J.L., K.N., S.B., T.P., and E.W.V. conducted the experimental design. O.K. advised on the experimental design. A.S.N., J.L., K.N., J.R.D., and A.H. performed the experiments. A.S.N., J.L., K.N., K.S., M.I.M., and E.W.V. conducted data interpretation. A.S.N., J.L., J.R.D., and E.W.V. wrote the manuscript.

ACKNOWLEDGMENTS

We are grateful to Kate Sutherland and Anton Berns for progenitor cell-directed adenoviruses, and Tomi Mäkelä and Ronald DePinho for *Lkb1*$^{fl/fl}$ mice. We thank the FIMM WebMicroscope team for scanning histological slides, the Laboratory Animal Centre for husbandry support, FuGU for expression profiling support, John-Patrick Mpindi for bioinformatics advice, Carolina Pereira and Virva Uotinen for technical support, and Panu Kovanen and Ori Brenner for histopathological guidance. Kate Sutherland is thanked for critical reading of the manuscript. Research was supported by the Innovative Medicines Initiative Joint Undertaking under grant agreement 115188 (IMI-PREDECT), resources of which are composed of financial contribution from the European Union's Seventh Framework Programme (FP7/2007-2013) and EFPIA companies in kind contribution (E.W.V.); the Sigrid Juselius and Orion-Farmos Foundations (E.W.V.); Finnish Cultural Foundation (00140509, J.L.); and University of Helsinki Doctoral Programme in Biomedicine scholarships (A.S.N. and J.L.).

Received: July 9, 2015
Revised: October 11, 2016
Accepted: December 19, 2016
Published: January 17, 2017

REFERENCES

Asselin-Labat, M.L., and Filby, C.E. (2012). Adult lung stem cells and their contribution to lung tumourigenesis. Open Biol. *2*, 120094.

Au, N.H., Gown, A.M., Cheang, M., Huntsman, D., Yorida, E., Elliott, W.M., Flint, J., English, J., Gilks, C.B., and Grimes, H.L. (2004). P63 expression in lung carcinoma: a tissue microarray study of 408 cases. Appl. Immunohistochem. Mol. Morphol. *12*, 240–247.

Bardeesy, N., Sinha, M., Hezel, A.F., Signoretti, S., Hathaway, N.A., Sharpless, N.E., Loda, M., Carrasco, D.R., and DePinho, R.A. (2002). Loss of the Lkb1 tumour suppressor provokes intestinal polyposis but resistance to transformation. Nature *419*, 162–167.

Boers, J.E., Ambergen, A.W., and Thunnissen, F.B. (1999). Number and proliferation of clara cells in normal human airway epithelium. Am. J. Respir. Crit. Care Med. *159*, 1585–1591.

Brahmer, J., Reckamp, K.L., Baas, P., Crinò, L., Eberhardt, W.E., Poddubskaya, E., Antonia, S., Pluzanski, A., Vokes, E.E., Holgado, E., et al. (2015). Nivolumab versus Docetaxel in advanced squamous-cell non-small-cell lung cancer. N. Engl. J. Med. *373*, 123–135.

Calles, A., Sholl, L.M., Rodig, S.J., Pelton, A.K., Hornick, J.L., Butaney, M., Lydon, C., Dahlberg, S.E., Oxnard, G.R., Jackman, D.M., and Jänne, P.A. (2015). Immunohistochemical loss of LKB1 is a biomarker for more aggressive biology in KRAS-mutant lung adenocarcinoma. Clin. Cancer Res. *21*, 2851–2860.

Cancer Genome Atlas Research Network (2012). Comprehensive genomic characterization of squamous cell lung cancers. Nature *489*, 519–525.

Chen, D.S., and Mellman, I. (2013). Oncology meets immunology: the cancer-immunity cycle. Immunity *39*, 1–10.

Chen, Z., Fillmore, C.M., Hammerman, P.S., Kim, C.F., and Wong, K.K. (2014). Non-small-cell lung cancers: a heterogeneous set of diseases. Nat. Rev. Cancer *14*, 535–546.

Cortez-Retamozo, V., Etzrodt, M., Newton, A., Rauch, P.J., Chudnovskiy, A., Berger, C., Ryan, R.J., Iwamoto, Y., Marinelli, B., Gorbatov, R., et al. (2012). Origins of tumor-associated macrophages and neutrophils. Proc. Natl. Acad. Sci. USA *109*, 2491–2496.

Gridelli, C., Rossi, A., Carbone, D.P., Guarize, J., Karachaliou, N., Mok, T., Petrella, F., Spaggiari, L., and Rosell, R. (2015). Non-small-cell lung cancer. Nat. Rev. Dis. Primers *1*, 15009.

Han, X., Li, F., Fang, Z., Gao, Y., Li, F., Fang, R., Yao, S., Sun, Y., Li, L., Zhang, W., et al. (2014). Transdifferentiation of lung adenocarcinoma in mice with Lkb1 deficiency to squamous cell carcinoma. Nat. Commun. *5*, 3261.

Heim, D., Budczies, J., Stenzinger, A., Treue, D., Hufnagl, P., Denkert, C., Dietel, M., and Klauschen, F. (2014). Cancer beyond organ and tissue specificity: next-generation-sequencing gene mutation data reveal complex genetic similarities across major cancers. Int. J. Cancer *135*, 2362–2369.

Jackson, E.L., Willis, N., Mercer, K., Bronson, R.T., Crowley, D., Montoya, R., Jacks, T., and Tuveson, D.A. (2001). Analysis of lung tumor initiation and progression using conditional expression of oncogenic K-ras. Genes Dev. *15*, 3243–3248.

Ji, H., Ramsey, M.R., Hayes, D.N., Fan, C., McNamara, K., Kozlowski, P., Torrice, C., Wu, M.C., Shimamura, T., Perera, S.A., et al. (2007). LKB1 modulates lung cancer differentiation and metastasis. Nature *448*, 807–810.

Jiang, L., Zhu, W., Streicher, K., Morehouse, C., Brohawn, P., Ge, X., Dong, Z., Yin, X., Zhu, G., Gu, Y., et al. (2014). Increased IR-A/IR-B ratio in non-small cell lung cancers associates with lower epithelial-mesenchymal transition signature and longer survival in squamous cell lung carcinoma. BMC Cancer *14*, 131.

Joshi, N.S., Akama-Garren, E.H., Lu, Y., Lee, D.Y., Chang, G.P., Li, A., DuPage, M., Tammela, T., Kerper, N.R., Farago, A.F., et al. (2015). Regulatory T cells in tumor-associated tertiary lymphoid structures suppress anti-tumor T cell responses. Immunity *43*, 579–590.

Kanazawa, H., Ebina, M., Ino-Oka, N., Shimizukawa, M., Takahashi, T., Fujimura, S., Imai, T., and Nukiwa, T. (2000). Transition from squamous cell carcinoma to adenocarcinoma in adenosquamous carcinoma of the lung. Am. J. Pathol. *156*, 1289–1298.

Kim, C.F., Jackson, E.L., Woolfenden, A.E., Lawrence, S., Babar, I., Vogel, S., Crowley, D., Bronson, R.T., and Jacks, T. (2005). Identification of bronchioalveolar stem cells in normal lung and lung cancer. Cell *121*, 823–835.

Koivunen, J.P., Kim, J., Lee, J., Rogers, A.M., Park, J.O., Zhao, X., Naoki, K., Okamoto, I., Nakagawa, K., Yeap, B.Y., et al. (2008). Mutations in the LKB1 tumour suppressor are frequently detected in tumours from Caucasian but not Asian lung cancer patients. Br. J. Cancer *99*, 245–252.

Koyama, S., Akbay, E.A., Li, Y.Y., Aref, A.R., Skoulidis, F., Herter-Sprie, G.S., Buczkowski, K.A., Liu, Y., Awad, M.M., Denning, W.L., et al. (2016). STK11/LKB1 deficiency promotes neutrophil recruitment and proinflammatory cytokine production to suppress T-cell activity in the lung tumor microenvironment. Cancer Res. *76*, 999–1008.

Kuner, R., Muley, T., Meister, M., Ruschhaupt, M., Buness, A., Xu, E.C., Schnabel, P., Warth, A., Poustka, A., Sültmann, H., and Hoffmann, H. (2009). Global gene expression analysis reveals specific patterns of cell junctions in non-small cell lung cancer subtypes. Lung Cancer *63*, 32–38.

Landvik, N.E., Hart, K., Skaug, V., Stangeland, L.B., Haugen, A., and Zienolddiny, S. (2009). A specific interleukin-1B haplotype correlates with high levels of IL1B mRNA in the lung and increased risk of non-small cell lung cancer. Carcinogenesis *30*, 1186–1192.

Leeman, K.T., Fillmore, C.M., and Kim, C.F. (2014). Lung stem and progenitor cells in tissue homeostasis and disease. Curr. Top. Dev. Biol. *107*, 207–233.

Leslie, M. (2016). Immunity goes local. Science *352*, 21–23.

Li, F., Han, X., Li, F., Wang, R., Wang, H., Gao, Y., Wang, X., Fang, Z., Zhang, W., Yao, S., et al. (2015). LKB1 inactivation elicits a redox imbalance to modulate non-small cell lung cancer plasticity and therapeutic response. Cancer Cell *27*, 698–711.

Lin, C., Song, H., Huang, C., Yao, E., Gacayan, R., Xu, S.M., and Chuang, P.T. (2012). Alveolar type II cells possess the capability of initiating lung tumor development. PLoS ONE *7*, e53817.

Liu, J., Cho, S.N., Akkanti, B., Jin, N., Mao, J., Long, W., Chen, T., Zhang, Y., Tang, X., Wistub, I.I., et al. (2015). ErbB2 pathway activation upon Smad4 loss promotes lung tumor growth and metastasis. Cell Rep. *10*, 1599–1613.

Maeda, Y., Tsuchiya, T., Hao, H., Tompkins, D.H., Xu, Y., Mucenski, M.L., Du, L., Keiser, A.R., Fukazawa, T., Naomoto, Y., et al. (2012). Kras(G12D) and Nkx2-1 haploinsufficiency induce mucinous adenocarcinoma of the lung. J. Clin. Invest. *122*, 4388–4400.

Mainardi, S., Mijimolle, N., Francoz, S., Vicente-Dueñas, C., Sánchez-García, I., and Barbacid, M. (2014). Identification of cancer initiating cells in K-Ras driven lung adenocarcinoma. Proc. Natl. Acad. Sci. USA *111*, 255–260.

Malkoski, S.P., Cleaver, T.G., Thompson, J.J., Sutton, W.P., Haeger, S.M., Rodriguez, K.J., Lu, S.L., Merrick, D., and Wang, X.J. (2014). Role of PTEN in basal cell derived lung carcinogenesis. Mol. Carcinog. *53*, 841–846.

Marino, S., Vooijs, M., van Der Gulden, H., Jonkers, J., and Berns, A. (2000). Induction of medulloblastomas in p53-null mutant mice by somatic inactivation of Rb in the external granular layer cells of the cerebellum. Genes Dev. *14*, 994–1004.

McGranahan, N., Furness, A.J., Rosenthal, R., Ramskov, S., Lyngaa, R., Saini, S.K., Jamal-Hanjani, M., Wilson, G.A., Birkbak, N.J., Hiley, C.T., et al. (2016). Clonal neoantigens elicit T cell immunoreactivity and sensitivity to immune checkpoint blockade. Science *351*, 1463–1469.

Mok, T.S., and Loong, H.H. (2016). Are we ready for immune checkpoint inhibitors for advanced non-small-cell lung cancer? Lancet *387*, 1488–1490.

Mukhopadhyay, A., Berrett, K.C., Kc, U., Clair, P.M., Pop, S.M., Carr, S.R., Witt, B.L., and Oliver, T.G. (2014). Sox2 cooperates with Lkb1 loss in a mouse model of squamous cell lung cancer. Cell Rep. *8*, 40–49.

Munder, M., Schneider, H., Luckner, C., Giese, T., Langhans, C.D., Fuentes, J.M., Kropf, P., Mueller, I., Kolb, A., Modolell, M., and Ho, A.D. (2006). Suppression of T-cell functions by human granulocyte arginase. Blood *108*, 1627–1634.

Muzumdar, M.D., Tasic, B., Miyamichi, K., Li, L., and Luo, L. (2007). A global double-fluorescent Cre reporter mouse. Genesis *45*, 593–605.

Nakagawa, K., Yasumitu, T., Fukuhara, K., Shiono, H., and Kikui, M. (2003). Poor prognosis after lung resection for patients with adenosquamous carcinoma of the lung. Ann. Thorac. Surg. *75*, 1740–1744.

Raber, P., Ochoa, A.C., and Rodríguez, P.C. (2012). Metabolism of L-arginine by myeloid-derived suppressor cells in cancer: mechanisms of T cell suppression and therapeutic perspectives. Immunol. Invest. *41*, 614–634.

Rawlins, E.L., Okubo, T., Xue, Y., Brass, D.M., Auten, R.L., Hasegawa, H., Wang, F., and Hogan, B.L. (2009). The role of Scgb1a1+ Clara cells in the long-term maintenance and repair of lung airway, but not alveolar, epithelium. Cell Stem Cell *4*, 525–534.

Rock, J.R., Onaitis, M.W., Rawlins, E.L., Lu, Y., Clark, C.P., Xue, Y., Randell, S.H., and Hogan, B.L. (2009). Basal cells as stem cells of the mouse trachea and human airway epithelium. Proc. Natl. Acad. Sci. USA *106*, 12771–12775.

Ryckman, C., Vandal, K., Rouleau, P., Talbot, M., and Tessier, P.A. (2003). Proinflammatory activities of S100: proteins S100A8, S100A9, and S100A8/A9 induce neutrophil chemotaxis and adhesion. J. Immunol. *170*, 3233–3242.

Snyder, E.L., Watanabe, H., Magendantz, M., Hoersch, S., Chen, T.A., Wang, D.G., Crowley, D., Whittaker, C.A., Meyerson, M., Kimura, S., and Jacks, T. (2013). Nkx2-1 represses a latent gastric differentiation program in lung adenocarcinoma. Mol. Cell *50*, 185–199.

Sutherland, K.D., Proost, N., Brouns, I., Adriaensen, D., Song, J.Y., and Berns, A. (2011). Cell of origin of small cell lung cancer: inactivation of Trp53 and Rb1 in distinct cell types of adult mouse lung. Cancer Cell *19*, 754–764.

Sutherland, K.D., Song, J.Y., Kwon, M.C., Proost, N., Zevenhoven, J., and Berns, A. (2014). Multiple cells-of-origin of mutant K-Ras-induced mouse lung adenocarcinoma. Proc. Natl. Acad. Sci. USA *111*, 4952–4957.

Talmadge, J.E., and Gabrilovich, D.I. (2013). History of myeloid-derived suppressor cells. Nat. Rev. Cancer *13*, 739–752.

Travis, W.D., Brambilla, E., Noguchi, M., Nicholson, A.G., Geisinger, K., Yatabe, Y., Powell, C.A., Beer, D., Riely, G., Garg, K., et al.; American Thoracic Society (2011). International Association for the Study of Lung Cancer/American Thoracic Society/European Respiratory Society: international multidisciplinary classification of lung adenocarcinoma: executive summary. Proc. Am. Thorac. Soc. *8*, 381–385.

Travis, W.D., Brambilla, E., and Riely, G.J. (2013). New pathologic classification of lung cancer: relevance for clinical practice and clinical trials. J. Clin. Oncol. *31*, 992–1001.

Tu, S., Bhagat, G., Cui, G., Takaishi, S., Kurt-Jones, E.A., Rickman, B., Betz, K.S., Penz-Oesterreicher, M., Bjorkdahl, O., Fox, J.G., and Wang, T.C. (2008). Overexpression of interleukin-1beta induces gastric inflammation and cancer and mobilizes myeloid-derived suppressor cells in mice. Cancer Cell *14*, 408–419.

Turner, B.M., Cagle, P.T., Sainz, I.M., Fukuoka, J., Shen, S.S., and Jagirdar, J. (2012). Napsin A, a new marker for lung adenocarcinoma, is complementary and more sensitive and specific than thyroid transcription factor 1 in the differential diagnosis of primary pulmonary carcinoma: evaluation of 1674 cases by tissue microarray. Arch. Pathol. Lab. Med. *136*, 163–171.

Winslow, M.M., Dayton, T.L., Verhaak, R.G., Kim-Kiselak, C., Snyder, E.L., Feldser, D.M., Hubbard, D.D., DuPage, M.J., Whittaker, C.A., Hoersch, S., et al. (2011). Suppression of lung adenocarcinoma progression by Nkx2-1. Nature *473*, 101–104.

Xu, X., Rock, J.R., Lu, Y., Futtner, C., Schwab, B., Guinney, J., Hogan, B.L., and Onaitis, M.W. (2012). Evidence for type II cells as cells of origin of K-Ras-induced distal lung adenocarcinoma. Proc. Natl. Acad. Sci. USA *109*, 4910–4915.

Xu, C., Fillmore, C.M., Koyama, S., Wu, H., Zhao, Y., Chen, Z., Herter-Sprie, G.S., Akbay, E.A., Tchaicha, J.H., Altabef, A., et al. (2014a). Loss of Lkb1 and Pten leads to lung squamous cell carcinoma with elevated PD-L1 expression. Cancer Cell *25*, 590–604.

Xu, X., Huang, L., Futtner, C., Schwab, B., Rampersad, R.R., Lu, Y., Sporn, T.A., Hogan, B.L., and Onaitis, M.W. (2014b). The cell of origin and subtype of K-Ras-induced lung tumors are modified by Notch and Sox2. Genes Dev. *28*, 1929–1939.

Zheng, D., Yin, L., and Chen, J. (2014). Evidence for Scgb1a1(+) cells in the generation of p63(+) cells in the damaged lung parenchyma. Am. J. Respir. Cell Mol. Biol. *50*, 595–604.